Influence of toroidal rotation on resistive tearing modes in tokamaks

S. Wang and Z. W. Ma*

Institute for Fusion Theory and Simulation, Zhejiang University, Hangzhou 310027, China.

Abstract

Influence of toroidal equilibrium plasma rotation on m/n=2/1 resistive tearing modes is studied numerically using a 3D toroidal MHD code (CLT). It is found that the toroidal rotation with or without shear can suppress the tearing instability and the Coriolis effect in the toroidal geometry plays a dominant role on the rotation induced stabilization. For a high viscosity plasma ($\tau_R/\tau_V \gg 1$, where τ_R and τ_V represent resistive and viscous diffusion time, respectively.), the effect of the rotation shear combined with the viscosity appears to be stabilizing. For a low viscosity plasmas ($\tau_R/\tau_V \ll 1$), the rotation shear shows a destabilizing effect when the rotation is large.

Keywords: MHD instability, Tearing mode, Tokamak, Toroidal rotation

*) Corresponding author: zwma@zju.edu.cn

I. INTRODUCTION

Magnetohydrodynamic (MHD) stability, in general, exists in both laboratory and space plasma. In magnetic confinement fusion (MCF), various classes of MHD instability essentially make up the basis of almost all aspects of achievable plasma performance and determine the principal operational limits in fusion devices like tokamak.[1, 2] Since the ultimate limit is believed to be set by ideal MHD kink modes, the penultimate limit may arise from the resistive tearing instabilities. With finite plasma resistivity, magnetic field lines and plasma would be partial decoupled in a narrow layer of the plasma (around rational surfaces in a fusion device) where ideal MHD breaks down, thereby field lines are allowed to tear or reconnect and form magnetic islands.[3] Those MHD instabilities could break magnetic flux surfaces, degrade plasma confinement, and lead to disruption eventually. Therefore, the MHD instabilities pose an enormous threat to MCF experiments.

The avoidance or control and stabilizing of the tearing modes is a very critical issue to maintain

good plasma confinement for sustained high β (ratio of plasma pressure to magnetic field pressure) performance and steady-state operation in future magnetic confinement reactors, such as ITER. A great deal of efforts have been made both theoretically and experimentally to explore various methods to control this instability, such as using localized radio-frequency current drive or heating, or by the application of external helical current coils, etc.[4, 5] In recent years, it has been experimentally observed from several tokamaks that neoclassical tearing modes (NTMs)[6, 7] would be destabilized when the plasma rotation is reduced.[8-10] It is indicated that the existence of toroidal shear flows may suppress development of the tearing mode stability. Plasma rotation is widely prevalent in tokamak devices and is usually resulted from neutral beams injection, ion cyclotron heating and self-consistent drift turbulence, etc. It has been known that toroidal plasma rotation can have a considerable effect on the stability of a tokamak.[11]

The influence of shear flows on tearing modes has been investigated for a long time. But most of past studies in theoretical analysis and numerical simulations were carried out in slab or cylindrical (large aspect ratio) geometries with a purely poloidal flow or a helical flow configuration.[12-17] Recently, R. Coelho and E. Lazzaro[18] studied the effect of sheared equilibrium plasma rotation on the stability of tearing modes in a cylindrical geometry quite elaborately by means of numerical MHD simulations. It is found that toroidal shear flow reduces the growth rates for viscous plasmas ($\tau_R/\tau_V>1$), but has a destabilizing effect for low viscosity plasmas ($\tau_R/\tau_V<<1$). D. Chandra $et.\ al$ [19] numerically investigated the influence of toroidal sheared equilibrium flows on both the classical and the neoclassical tearing mode in a toroidal geometry by using NEAR code which solves a set of generalized reduced MHD equations. While differential rotation between rational (q=m/n) magnetic surfaces without shear is found to be stabilizing, toroidal velocity shear at the resonant surface is shown to be destabilizing in the absence of perpendicular viscous diffusion. A. Sen $et.\ al$ [20] derived a flow modified external kink equation for a single helicity mode in a toroidal geometry and found the corrections to the tearing mode stability index Δ' arising from toroidal shear flow contributions. In their results, toroidal shear flow is also seen to make a destabilizing contribution to the tearing mode.

A new initial value MHD code (CLT) in toroidal geometries is developed to study the MHD stabilities in toroidal devices. In this paper, we use CLT to examine the influence of rotation on the tearing modes. This paper is organized as follows. In Sec. II, the formulation of CLT including the MHD

equations and numerical methods is presented. Benchmarks of CLT are shown in Sec. III. Sec. IV gives the simulation results for m/n=2/1 resistive tearing modes with different rotation speeds and shear profiles. Finally, conclusion and discussion are placed in Sec. V.

II. BASIC EQUATIONS FOR CLT

The full set of resistive MHD equations including dissipations is given as follows,

$$\partial_t \rho = -\nabla \cdot (\rho \mathbf{v}) + \nabla \cdot [D\nabla(\rho - \rho_0)], \tag{1}$$

$$\partial_t p = -\mathbf{v} \cdot \nabla p - \Gamma p \nabla \cdot \mathbf{v} + \nabla \cdot [\kappa \nabla(p - p_0)], \tag{2}$$

$$\partial_t \mathbf{v} = -\mathbf{v} \cdot \nabla \mathbf{v} + (\mathbf{J} \times \mathbf{B} - \nabla p)/\rho + \nabla \cdot [\nu \nabla(\mathbf{v} - \mathbf{v}_0)], \tag{3}$$

$$\partial_t \mathbf{B} = -\nabla \times \mathbf{E}, \tag{4}$$

with

$$\mathbf{E} = -\mathbf{v} \times \mathbf{B} + \eta(\mathbf{J} - \mathbf{J}_0), \tag{5}$$

$$\mathbf{J} = \nabla \times \mathbf{B}, \tag{6}$$

where ρ, p, $\mathbf{v}$, $\mathbf{B}$, $\mathbf{E}$, $\mathbf{J}$ are the plasma density, thermal pressure, plasma velocity, magnetic field, electric field, and current density, respectively. $\Gamma(=5/3)$ is the ratio of specific heat of plasma. All variables are normalized as follows: $\mathbf{B}/B_{00} \rightarrow \mathbf{B}$, $\mathbf{x}/a \rightarrow \mathbf{x}$, $\rho/\rho_{00} \rightarrow \rho$, $\mathbf{v}/v_A \rightarrow \mathbf{v}$, $t/\tau_a \rightarrow t$, $p/(B_{00}^2/\mu_0) \rightarrow p$, $\mathbf{J}/(B_{00}/\mu_0 a) \rightarrow \mathbf{J}$, $\mathbf{E}/(v_A B_{00}) \rightarrow \mathbf{E}$, $\eta/(\mu_0 a^2/\tau_a) \rightarrow \eta$, where $\tau_a = a/v_A$ is the Alfvénic time, $v_A = B_{00}/(\mu_0 \rho_{00})^{1/2}$ is the Alfvénic speed, B_{00} and ρ_{00} are the magnetic field and plasma density at the magnetic axis, respectively, and a is the half size of the plasma cross-section in the Z=0 plane.

For the equilibrium, following equations should be satisfied:

$$\nabla \cdot (\rho_0 \mathbf{v}_0) = 0, \tag{7}$$

$$\mathbf{v}_0 \cdot \nabla p_0 + \Gamma p_0 \nabla \cdot \mathbf{v}_0 = 0, \tag{8}$$

$$\rho_0 \mathbf{v}_0 \cdot \nabla \mathbf{v}_0 = \mathbf{J}_0 \times \mathbf{B}_0 - \nabla p_0, \tag{9}$$

and

$$\nabla \times \mathbf{E}_0 = 0. \tag{10}$$

Substituting these equilibrium equations into Equations (1-4), Equations (1-4) can be rewritten as

$$\partial_t \rho = -\nabla \cdot (\rho \mathbf{v}_1 + \rho_1 \mathbf{v}_0) + \nabla \cdot [D\nabla(\rho - \rho_0)], \tag{11}$$

$$\partial_t p = -\mathbf{v}_1 \cdot \nabla p - \mathbf{v}_0 \cdot \nabla p_1 - \Gamma(p\nabla \cdot \mathbf{v}_1 + p_1 \nabla \cdot \mathbf{v}_0) + \nabla \cdot [\kappa \nabla(p - p_0)], \tag{12}$$

$$\partial_t \mathbf{v} = -(\mathbf{v} \cdot \nabla \mathbf{v}_1 + \mathbf{v}_1 \cdot \nabla \mathbf{v}_0 + \rho_1 \mathbf{v}_0 \cdot \nabla \mathbf{v}_0 / \rho) + (\mathbf{J}_1 \times \mathbf{B} + \mathbf{J}_0 \times \mathbf{B}_1 - \nabla p_1)/\rho + \nabla \cdot (\nu \nabla \mathbf{v}_1), \tag{13}$$

$$\partial_t \mathbf{B} = -\nabla \times \mathbf{E}_1, \tag{14}$$

where the variables with subscript 0 represent equilibrium components and 1 for perturbation components, e.g. $\mathbf{v}_1 = \mathbf{v} - \mathbf{v}_0$. Thus, numerical errors from equilibrium can be minimized.

In CLT, a cylindrical coordinate system (R, φ, Z) as shown in Figure 1 is used to solve Equations (11-14). In a toroidal geometry device like tokamak, R, φ, and Z indicate major radius, toroidal, and up-down directions, respectively. One advantage of this coordinate system is that one can avoid the singularity near r=0 point that occurs in the toroidal coordinate (ψ, θ, ζ). However, the outer boundary handling would be more difficult in cylindrical coordinate. In the current version of CLT, the plasma boundary at the last flux surface of plasma is assumed to be fixed.
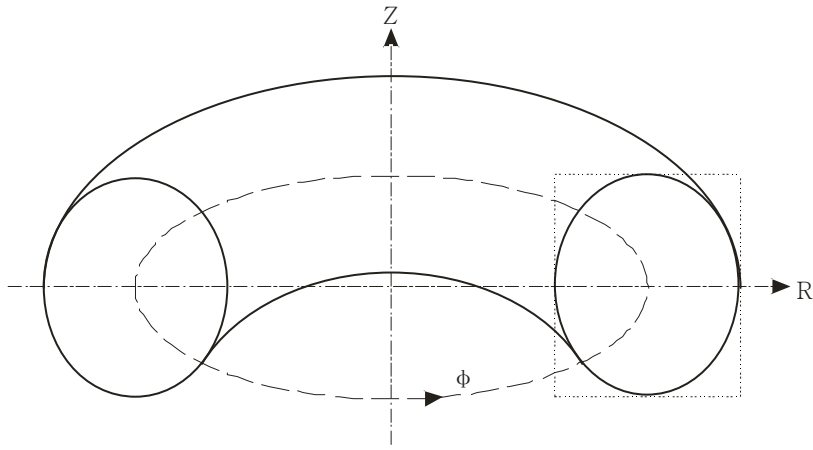
FIG. 1. Sketch of cylindrical coordinate system (R, φ, Z) in a toroidal geometry device
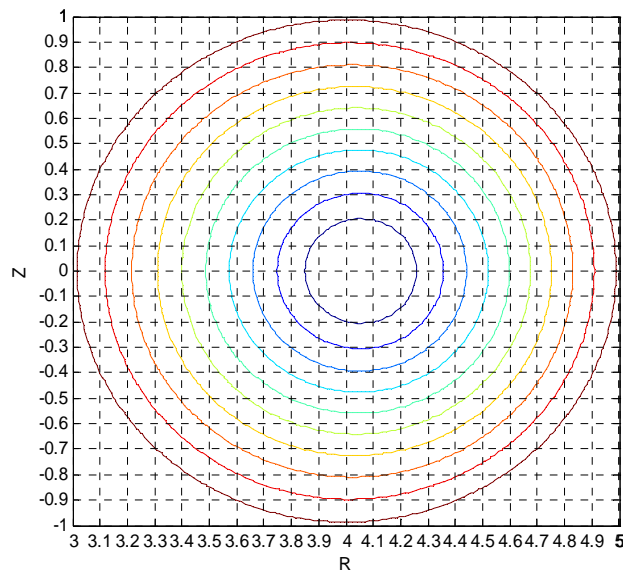
FIG. 2. Sketch of grids and flux surfaces in RZ-plane

The grids are dispersed in R, Z, φ direction and those are rectangular grids in RZ-plane as shown in Figure 2. Finite difference method is employed in the R and Z directions, while in the φ direction, either finite difference or pseudo-spectrum method is used. In the time-advance, 4th order Runge-Kutta scheme is chosen.

III. BENCHMARK STUDY

Benchmark tests are carried out to validate the credibility and applicability of CLT.

A. Internal kink mode

The first test case is the m/n=1/1 internal kink mode. The geometry of initial equilibrium is simply adopted a circular poloidal cross-section with an aspect ratio of 4.0. The safety factor is varied monotonously from q_0=0.6 at the center to q_a=2.5 on the edge as shown in Figure 3 where the pressure profile is also shown. The q = m/n = 2 singular surface is located at about $r \equiv (\psi_{norm})^{1/2}$ =0.63, with ψ_{norm} the normalized poloidal flux, and the peak β is chosen to range from 0.027 to 0.164 for scaling study. The ideal MHD m/n=1/1 internal kink modes are unstable in these equilibriums.

The initial equilibrium variables such as magnetic fields and currents in CLT are from NOVA code[21]. The mode structure and linear growth rate of the internal kink mode for the given equilibrium can be also obtained from the NOVA code. In this case, the resistivity is set to be zero while small values ($\sim 10^{-6}$) for the viscosity and thermal conductivity is used to keep numerically stable in the CLT simulations.

Figure 4 shows the 2D structure of the eigen function (flux-surface normal velocity ($\mathbf{v} \cdot \nabla \psi$)) from a CLT simulation with β_0=0.057. A dominant m=1 mode can be seen. Relevant mode structures versus major radius R in the mid-plane Z=0 of the cross-section (the dot-line in Figure 4) are shown in Figure 5. The dotted line is obtained from CLT and the dashed one is from NOVA. It is evident that the two results are in a good agreement.

Linear growth rates of the ideal kink mode with different β are shown in Figure 6. The linear growth rates from both CLT (red hollow dots) and NOVA (blue solid dots) increase with increase of β. When β is small, the growth rates from the two codes agree quite well; while β becomes larger, the growth rates from CLT are a bit smaller than that from NOVA. This may be attributed to that the CLT

simulations are not completely 'ideal' actually, because of retaining of small dissipative terms and other numerical dissipations.
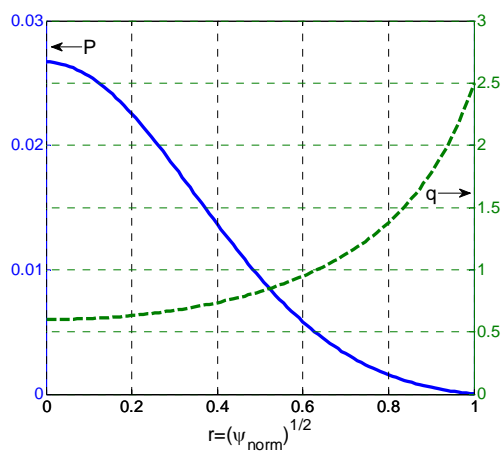
FIG. 3. Initial equilibrium profiles of P and q for m/n=1/1 internal kink mode simulation.
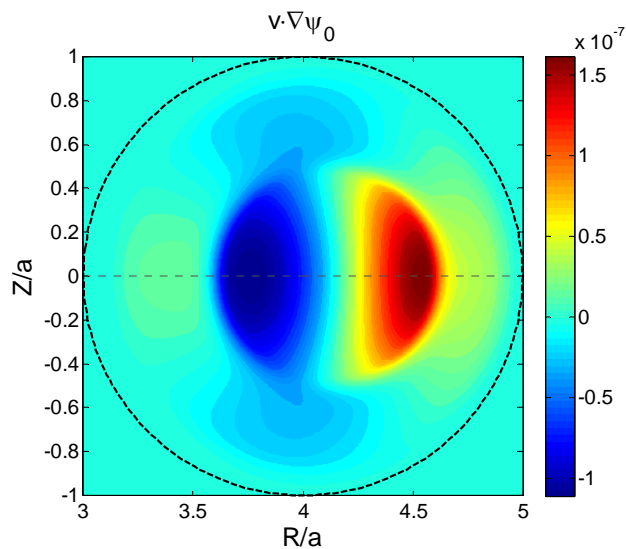
FIG. 4. Color contour plot of the internal kink mode structure; the flux-surface normal velocity ($\mathbf{v} \cdot \nabla \psi$) is shown.
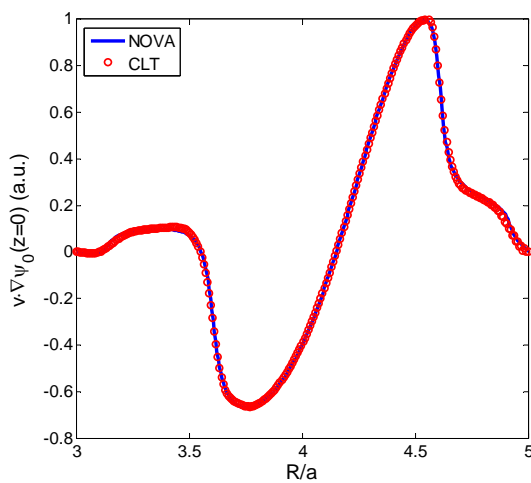
FIG. 5. Eigen function vs. R in mid-plane from CLT (hollow dots) compared with that from NOVA (dish line)
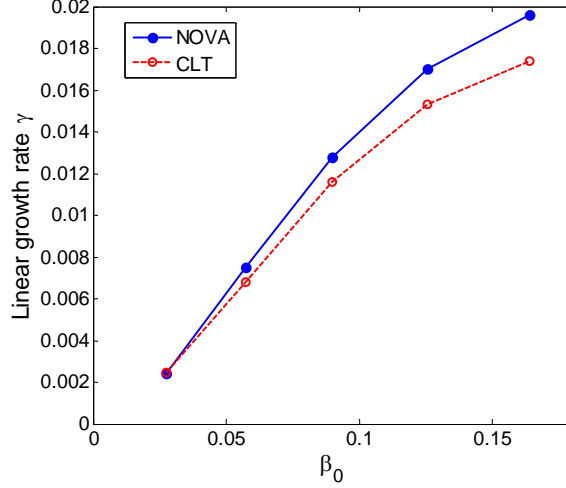
FIG. 6. Linear growth rates with different β (red hollow dots from CLT and blue solid dots from NOVA)

B. Resistive tearing/kink mode

The second test case is the m/n=2/1 resistive tearing mode. The geometry is given as the same as above, while the safety factor q varies from 1.6 at the center to 7.8 at the edge as shown in Figure 7. β is chosen to be low enough to avoid a ballooning instability. The m/n=2/1 mode is usually dominant with finite resistivity for such equilibrium.

Figure 8a shows the structure of the eigen function (perturbations of toroidal electric field $E_{\varphi 1}$) from CLT with normalized resistivity $\eta=10^{-5}$. The main perturbation is localized around the q=2 surface with dominant poloidal mode number m=2, which is expected from analytical theory. Relevant Poincare plot of magnetic field lines is shown in Figure 8b.

A series of cases for different resistivities is conducted. The relation between linear growth rates and Lundquist numbers S is shown in Figure 9. The fitting of the scaling low is about $\gamma \propto S^{-0.603}$ that agrees quite well with the analytical result[22], $\gamma \propto S^{-3/5}$.
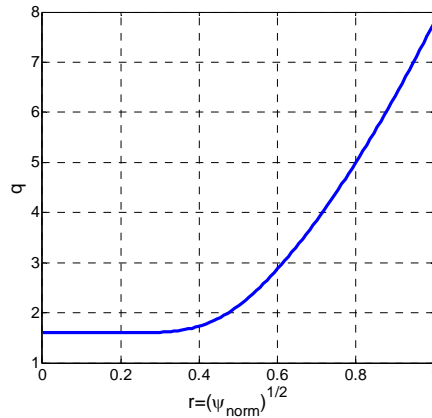
FIG. 7. Initial equilibrium q profile for m/n=2/1 resistive tearing mode simulation.
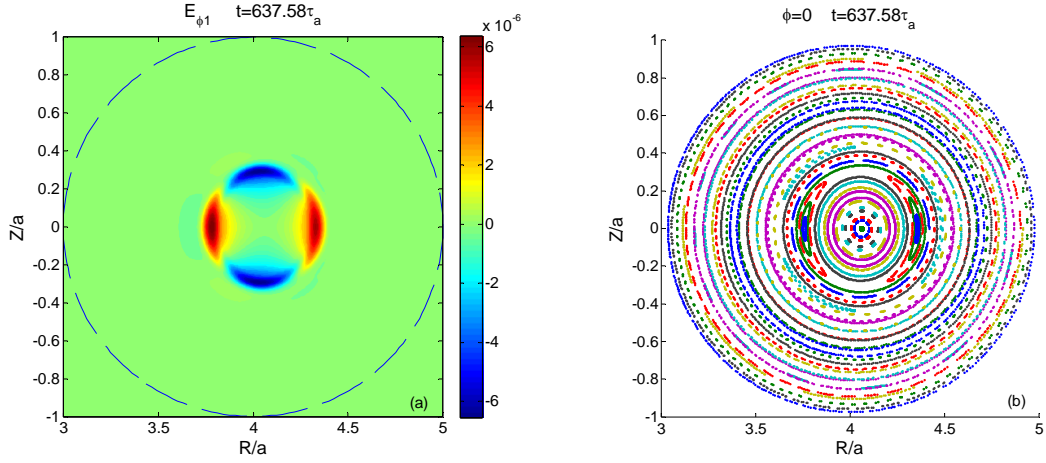
FIG. 8. (a) Mode structure and (b) Poincare plot of magnetic field lines for m/n=2/1 resistive tearing mode with $\eta=10^{-5}$
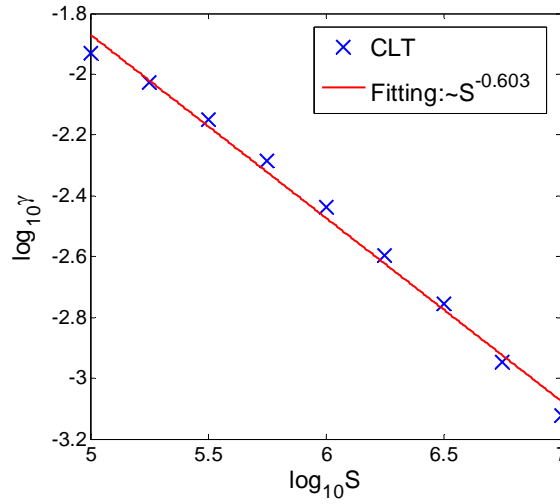
FIG. 9. Scaling of linear growth rates γ vs. Lundquist numbers S for m/n=2/1 resistive tearing mode

The m/n=1 resistive kink mode with $\eta=10^{-5}$ is also shown in Figure 11 with q-profile given in Figure 10. The scaling of γ about S is fitted as $\gamma\propto S^{-0.332}$ shown in Figure 12, which also agrees well with the analytical prediction[23] ($\gamma\propto S^{-1/3}$) and previous simulation results[24-26].
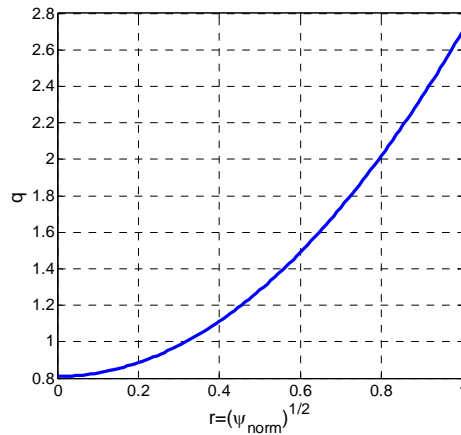
FIG. 10. Initial equilibrium q profile for m/n=1/1 resistive kink mode simulation.
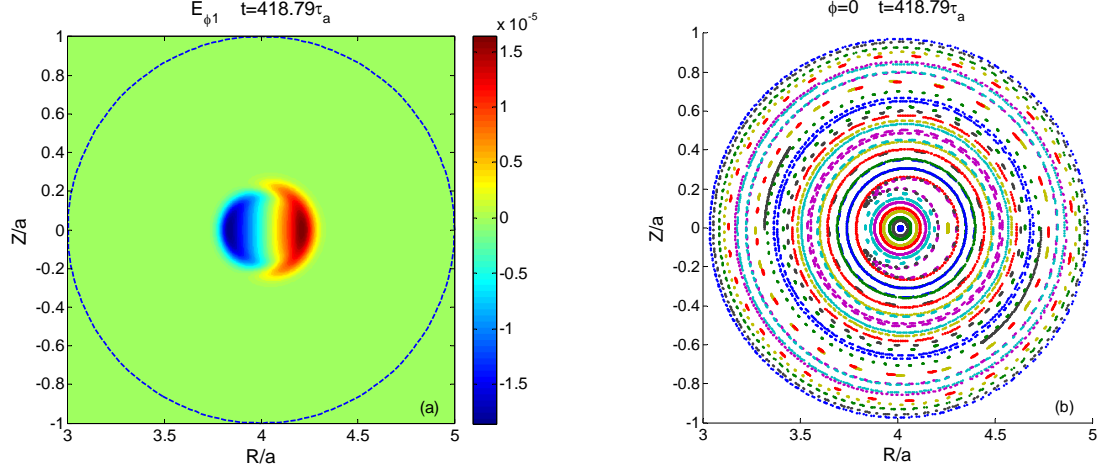
FIG. 11. (a) Mode structure and (b) Poincare plot of magnetic field lines for m/n=1/1 resistive kink mode with $\eta=10^{-5}$
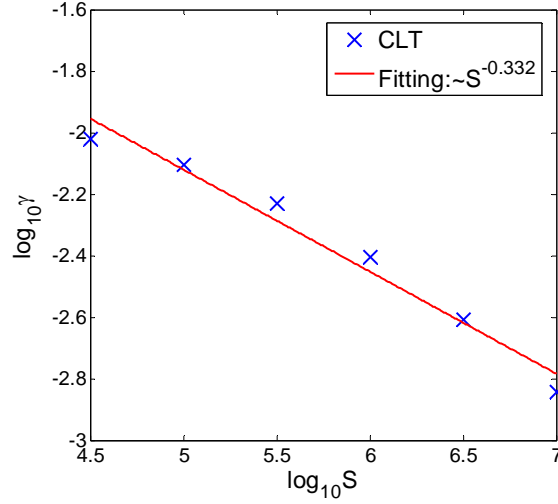
FIG. 12. Scaling of linear growth rates γ vs. Lundquist numbers S for m/n=1/1 resistive kink mode

IV. TEARING MODE WITH TOROIDAL ROTATION

Benchmark results have confirmed the reliability of CLT. We then use it to study resistive tearing modes with equilibrium toroidal rotation.

The equilibrium with toroidal flow can be solved by a modified Grad-Shafranov equation:

$$\Delta^* \psi \equiv R^2 \nabla \cdot \left(\frac{1}{R^2} \nabla \psi \right) = -g \frac{dg}{d\psi} - \mu_0 R^2 \left. \frac{\partial P}{\partial \psi} \right|_R , \qquad (15)$$

where the pressure $P = P(\psi, R)$ is no longer a function of the flux surface and satisfies the relation $\partial_R P|_\psi = \rho R \Omega^2$. The frequency of the toroidal rotation Ω can be proved a function of the flux surface ($\Omega = \Omega(\psi)$) from $\partial_t \mathbf{B}_0 = \nabla \times (\mathbf{u}_0 \times \mathbf{B}_0) = 0$. In general, the equilibrium plasma temperature T is still assumed to be a function of the flux surface, i.e. $T = T(\psi)$. Then from $\mathbf{B}_0 \cdot \nabla T = 0$, the pressure can be

simply expressed as $P = P_s(\psi)\exp[m\Omega^2(R^2 - R_m^2)/2T]$, where $P_s(\psi) = \rho_s(\psi)T(\psi)/m$ is the pressure without plasma flow, $\rho_s(\psi)$ is the stationary equilibrium density and R_m is the major radius at the magnetic axis. The density of equilibrium with toroidal flow can be written as $\rho = mP/T = \rho_s(\psi)\exp[m\Omega^2(R^2 - R_m^2)/2T]$.

The q-profile is chosen as the same as Figure 7, i.e., the dominant tearing mode is m/n=2/1. The plasma temperature T is chosen to be uniform. Three rotation profiles are adopted as shown in Figure 13. All of them have the same frequency ($\Omega_2 \equiv \Omega(r_2)$, where $r_2 = r|_{q=2}$) at the q=2 surface but different toroidal rotation shear ($\Omega_2' \equiv d\Omega/dr(r_2)$). The frequency of toroidal rotation is chosen to be constant for Profile 1, which is used to study the pure rotation effect without shear. Profile 2 has a shear about $\Omega_2'/\Omega_2 \approx -1.2$ around the q=2 surface, while Profile 3 is for a larger shear $\Omega_2'/\Omega_2 \approx -3.6$, as a comparison, the magnetic shear ($q'/q(r_2)$) at the q=2 surface is about 2.5 in the equilibrium. Ω_2 varies from 0 to 0.0074($\omega_A = v_A/a$). The normalized resistivity η and viscosity υ are fixed to $1.0*10^{-5}$ and $1.0*10^{-6}$, respectively. Since $\tau_R/\tau_V \ll 1$, the plasma is usually referred to be a low viscosity plasma.
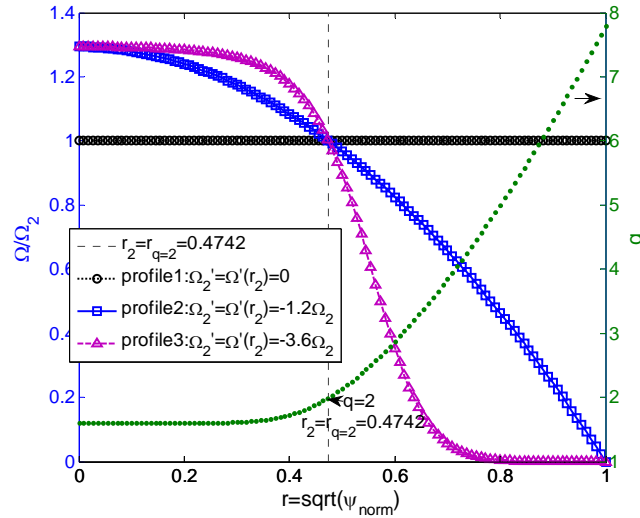
FIG. 13. Equilibrium toroidal rotation Ω profiles
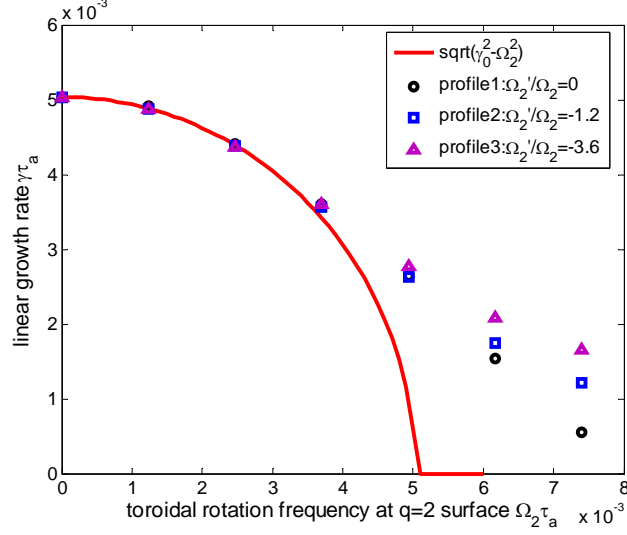
FIG. 14. Linear growth rates γ vs. toroidal rotation at q=2 surface Ω_2

Table 1. Summary of contributions of various terms in CLT on the linear growth rate of tearing modes.

Rotation Ω_2	Equilibrium pressure used	Evolution of density	Linear growth rate
0	$P_0 = P_s(\psi)$	Off	0.00504
0	$P_0 = P_s(\psi)$	On	0.00504
0.00247	$P_0 = P_s(\psi)$	Off	0.00463
0.00247	$P_0 = P_s(\psi)\mathrm{e}^{\frac{m\Omega^2(R^2-R_m^2)}{2T}}$	Off	0.00461
0.00247	$P_0 = P_s(\psi)$	On	0.00443
0.00247	$P_0 = P_s(\psi)\mathrm{e}^{\frac{m\Omega^2(R^2-R_m^2)}{2T}}$	On	0.00441

In the paper, we mainly focus on the influence of toroidal rotation on the linear stage of the m/n=2/1 resistive tearing modes, i.e. the influence on linear growth rate of the modes.

As shown in Figure 14, the linear growth rates of the mode decrease with Ω_2 increase for all of three profiles. Unlike that in cylindrical geometry[18], an equilibrium toroidal plasma in toroidal geometry flow not only provides a propagating frequency to the tearing mode, but also affects its growth rate even if the rotation is uniform. Comparing the results from the three different Ω profiles under the same rotation frequency at the q=2 surface (Ω_2), the difference of the growth rates among the three cases can be negligible when Ω_2 is rather small. But, when Ω_2 becomes large, we can see the linear growth rates with a shear rotation (Profile 2 and 3) are larger than that with a uniform rotation (Profile 1). The growth rate becomes larger as the gradient of the rotation shear increases, which suggests that a uniform

rotation leads to a stronger stabilizing effect when the rotation is sufficiently strong. It means that under condition of such equilibriums and parameters, the stabilizing effect on the tearing mode may be primarily resulted from the rotation itself, whereas rotation shear devotes an opposite contribution. It is quite consistent with the results from Ref. 18, 19, and 20 about the destabilizing effect of rotation shear for low viscosity plasmas.

As investigation in Ref. 19 for differential flows, the source of the stabilizing influence of rotation has been primarily traced to the pressure-curvature term and the toroidal coupling. But in our study, since a constant Ω in Profile 1 is used, we can exclude the effect of the toroidal mode coupling on the flow induced stabilization. Although the toroidal flow causes the modification of the equilibrium pressure from $P_s(\psi)$ to $P_s(\psi)\exp[m\Omega^2(R^2 - R_m^2)/2T]$, the modification can be ignored since $R^2\Omega^2 << T/m$. It is suggested that the pressure-curvature term does not play a role on the stabilization. For further verification, we artificially adopt the stationary equilibrium pressure $P_s(\psi)$ instead of the pressure with flow induced modification. As indicated in Table 1, the linear growth rate only has a little change for the pressure with considering the modification of the toriodal rotation, but is much smaller than that without flow. It means that equilibrium modifications of the pressure profile caused by the centrifugal effects of flow have a little stabilizing effect but not sufficient. There should be other physical mechanism for the stabilization induced by the rotation flow. The following analytical estimation is useful to obtain the answer.

According to the theory of Frieman and Rotenberg[27], the linear equation about Lagrangian displacement vector ξ for ideal MHD with an equilibrium flow $\mathbf{U}$ can be written as

$$\rho\partial_t^2\xi + 2\rho(\mathbf{U}\cdot\nabla)\partial_t\xi = \mathbf{F}(\xi) = \mathbf{F}_s(\xi) + \nabla\cdot(\rho\xi\mathbf{U}\cdot\nabla\mathbf{U} - \rho\mathbf{U}\mathbf{U}\cdot\nabla\xi), \tag{16}$$

where $\mathbf{F}_s(\xi) = \nabla(\Gamma P\nabla\cdot\xi + \xi\cdot\nabla P) + (\nabla\times\mathbf{B})\times\nabla\times(\xi\times\mathbf{B}) + \nabla\times[\nabla\times(\xi\times\mathbf{B})]\times\mathbf{B}$ that is the component associated with a static equilibrium. If we consider a uniform toroidal rotation, i.e. $\mathbf{U} = R\Omega\hat{\mathbf{e}}_\phi$, Ω=constant, and ξ is assumed the form of a normal mode $\xi \sim e^{-i\tilde{\omega}t+in\phi}$, where $\tilde{\omega} = \omega + i\gamma$ is a complex frequency, ω and γ are the real frequency and the growth rate, respectively, Eq. (16) can be simplified as

$$-\rho(\tilde{\omega} - n\Omega)^2\xi - 2i\rho(\tilde{\omega} - n\Omega)\Omega(\hat{\mathbf{e}}_Z \times \xi) = \mathbf{F}_s(\xi) - \nabla\cdot(\rho\xi)R\Omega^2\hat{\mathbf{e}}_R. \tag{17}$$

It can be reduced to the familiar linear equation for static equilibrium when Ω=0,

$$-\rho\tilde{\omega}^2\xi = \mathbf{F}_s(\xi). \tag{18}$$

Comparing Eq. (17) to Eq. (18), besides a shift in frequency, the Coriolis effect as well as a centrifugal force $-\nabla \cdot (\rho \boldsymbol{\xi}) R \Omega^2 \hat{\mathbf{e}}_R$ appear in a second term on the left and right hands of Equation (17), respectively. These two terms would not appear in a cylindrical geometry with an equivalent toroidal flow. The stabilizing influence of the toroidal flow is only attributed to the centrifugal effect and Coriolis effect arising from toroidal geometry. Noting the centrifugal term is related to the perturbation of the density ($\rho_1 = -\nabla \cdot (\rho \boldsymbol{\xi})$), we can drop the centrifugal effect by turning off the density evolution in CLT, i.e., $\rho_1 = 0$ for all the time. In the absence of the flow, a little difference occurs whether $\rho_1 = 0$ as shown in Table 1. However, when the toroidal rotation presented, the linear growth rate appears larger without the density evolution than with the density evolution. It is suggested that the centrifugal effect also puts up a stabilizing influence. But the reduction of the linear growth rate is still quite considerable in the presence of the toroidal flow even if the centrifugal effect is dropped. It implies that the Coriolis effect may have a considerable even dominant contribution to stabilize the mode. To understand this mechanism, a rough estimation is given based on Equations (17) and (18). If we assume that the difference of the eigenfunction $\boldsymbol{\xi}$ is negligible with and without flow, i.e., $\mathbf{F}_s(\boldsymbol{\xi})$ in Equation (17) can be replaced by $\mathbf{F}_s(\boldsymbol{\xi})$ in Equation (18), and the centrifugal term is ignorable. Thus, Equation (18) is simplified as

$$-(\tilde{\omega} - n\Omega)^2 \boldsymbol{\xi} - 2i(\tilde{\omega} - n\Omega)\Omega(\hat{\mathbf{e}}_Z \times \boldsymbol{\xi}) \approx \gamma_0^2 \boldsymbol{\xi} . \tag{19}$$

where γ_0 is the growth rate of the mode without flow. In our cylindrical coordinate, Equation (19) can be written to a set of equations:

$$[(\tilde{\omega} - n\Omega)^2 + \gamma_0^2]\xi_R - i2(\tilde{\omega} - n\Omega)\Omega\xi_\phi = 0 , \tag{20a}$$

$$[(\tilde{\omega} - n\Omega)^2 + \gamma_0^2]\xi_\phi + i2(\tilde{\omega} - n\Omega)\Omega\xi_R = 0 . \tag{20b}$$

From Equation (20), the eigenvalue equation for $\tilde{\omega}$ is obtained:

$$[(\tilde{\omega} - n\Omega)^2 + \gamma_0^2]^2 - 4(\tilde{\omega} - n\Omega)^2 \Omega^2 = 0 . \tag{21}$$

To solve this eigenvalue equation, the growth rate of a growing mode with the rotation Ω can be attained as $\gamma = (\gamma_0^2 - \Omega^2)^{1/2}$. This relation is shown as a red solid curve in Figure 14. Although the resistivity and the correction to the pressure from the rotation have not been considered, the estimated growth rates agrees quite well with the simulation results, especially when $\Omega_2 < \gamma_0$ for all the three profiles. It indicates that the Coriolis effect devote a dominatingly stabilizing contribution to the tearing mode with toroidal rotation in a toroidal geometry at least when $\Omega_2 < \gamma_0$.
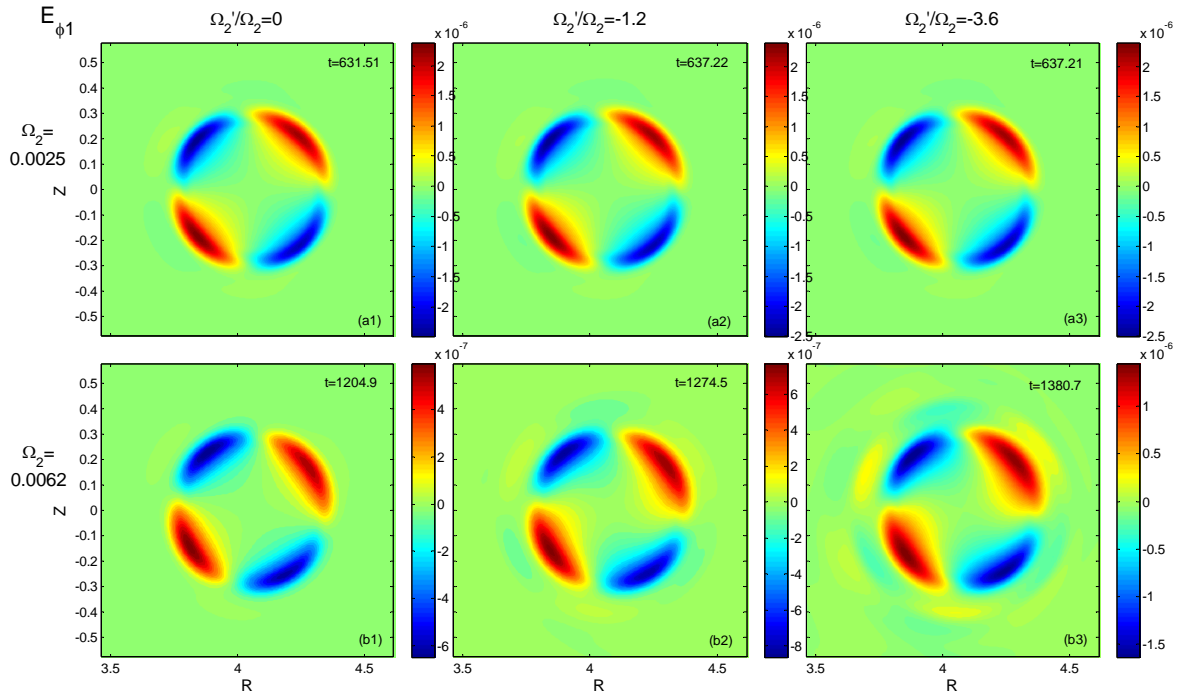
FIG. 15. Mode structures ($E_{\varphi 1}$) for different rotations and shears

Figure 15 shows the mode structures (perturbations of the toroidal electric field $E_{\varphi 1}$) at different Ω profiles (different shear) with $\Omega_2=0.0025$ and $\Omega_2=0.0062$, respectively. When the rotation is small ($\Omega_2=0.0025$), indeed, the mode structures differ little from that without flow in Figure 8a, besides some global shift. However, when the rotation is large ($\Omega_2=0.0062$) and sheared, the mode structure is distorted. The larger the shear is, the more severe the structure is distorted. Hence, this deformation of the mode structure or the magnetic island structure may be one of illustrations how local flow shear can influence the stability of the tearing mode as mentioned in Ref. 28 and 29.

Table 2 Linear growth rates of tearing modes for various viscosities and rotation shears.

Rotation shear	Linear growth rate $\gamma\tau_a$		
(Ω_2'/Ω_2)	$\nu_0=1*10^{-6}$	$\nu_0=1*10^{-5}$	$\nu_0=1*10^{-4}$
0	0.000841	0.000723	0.000349
-1.2	0.000857	0.000724	0.000343
-3.6	0.000866	0.000731	0.000336
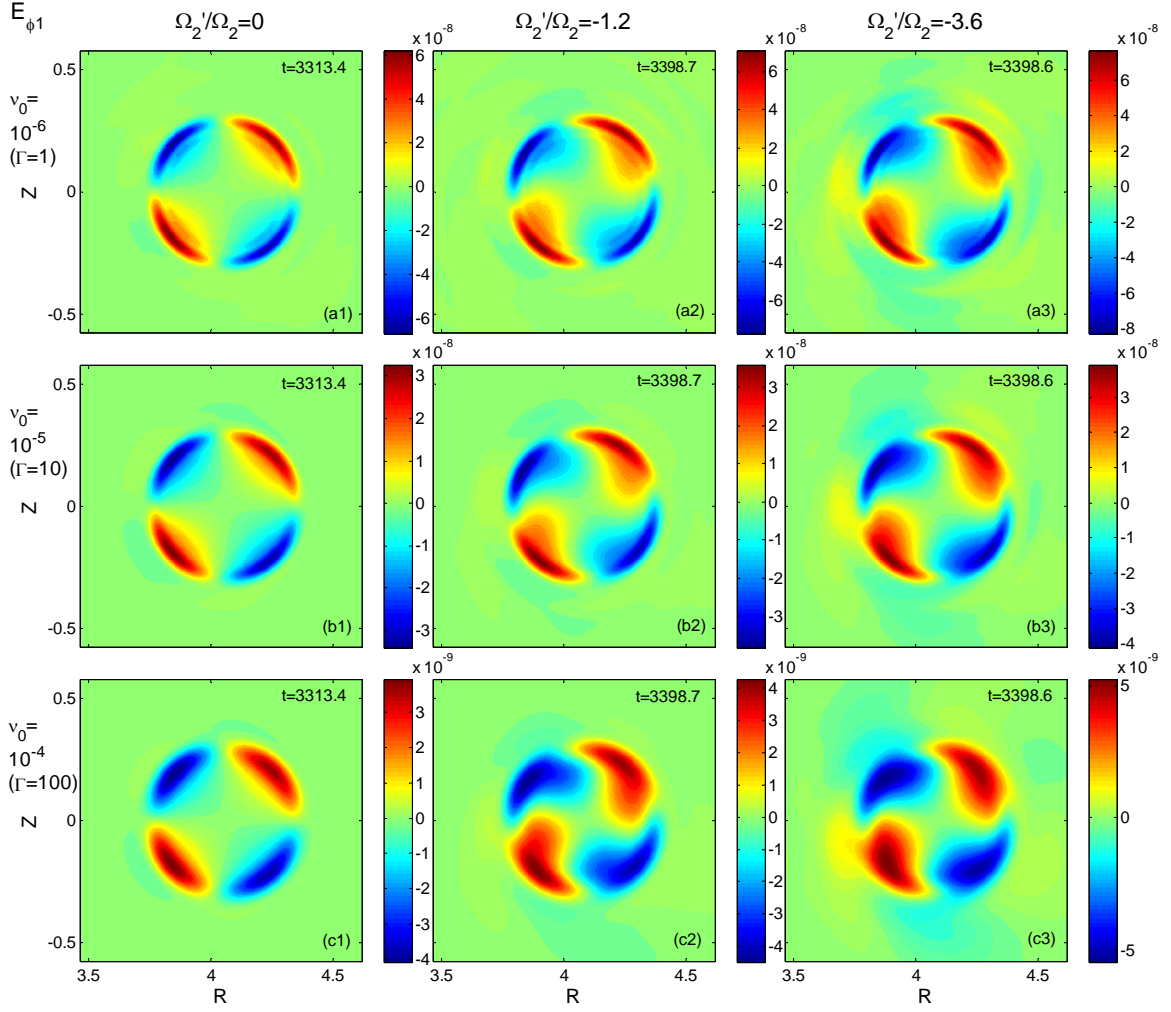
FIG. 16. Mode structures ($E_{\varphi 1}$) for different viscosities and rotation shears

The role of the viscosity is also examined. We fix Ω_2 as 0.0062 and choose the normalized resistivity η to be $1.0*10^{-6}$. The normalized viscosity ν_0 is chosen to be from $1.0*10^{-6}$ to $1.0*10^{-4}$. As shown in Table 2, the linear growth rate of the mode rapidly decreases with increase of the viscosity for all three rotation profiles. When the viscosity is small ($\nu_0=1*10^{-6}$), the linear growth rates increases with increase of the rotation shear, as demonstrated above. But, when the viscosity becomes large ($\nu_0=1*10^{-4}$), the linear growth rate decreases as the rotation shear increases. This is consistent with the results of Ref. 18 for viscous plasmas. For an intermediate viscosity ($\nu_0\sim1*10^{-5}$), the linear growth rate are nearly the same for different rotation shears. It implies that the rotation shear coupling with the viscosity may take a stabilizing effect, although the rotation shear itself plays a destabilizing role.

The mode structures for various viscosities and different rotation shears are shown in Figure 16 as well. It is evident that the distortion of the mode structure becomes more severe when the rotation shear increases. Meanwhile, a more severe distortion of the mode structure occurs with the higher viscosity

for the same rotation shear.
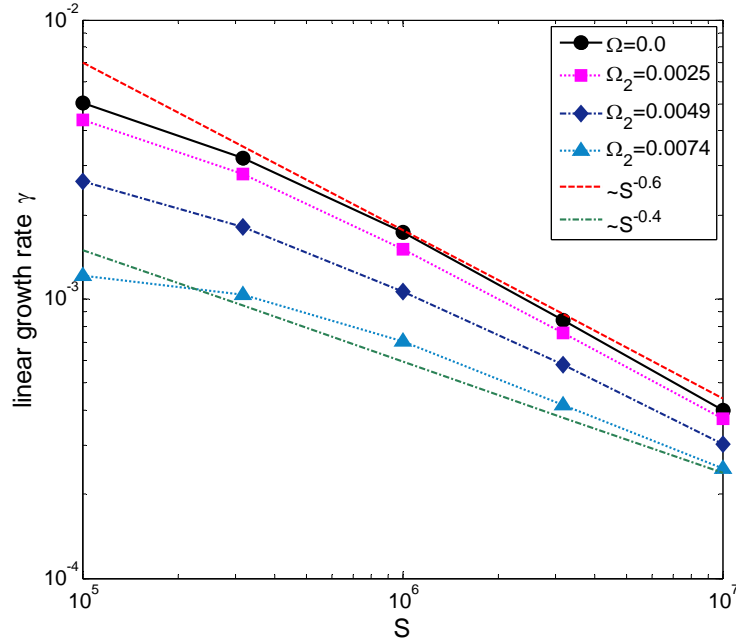
FIG. 17. Scaling of linear growth rates γ vs. Lundquist numbers S for different rotation Ω_2

We also study the relation between the linear growth rate γ of tearing modes and Lundquist number S under different rotations for Profile 2. As shown in Fig. 17, the log-log curve about γ versus S seems to flatten, i.e., the dependence of γ on S is weakened, when Ω_2 increased.

VII. CONCLUSION AND DISCUSSION

A new MHD code (CLT) in the toroidal geometry under the cylindrical coordinate system is developed to study the MHD stabilities. Through a series of the benchmark tests, it is indicated that CLT is feasible and reliable.

CLT is further used to examine the effect of toroidal plasma rotations on the resistive tearing mode in tokamaks. The simulation results show that, the toroidal rotation itself can suppress the tearing instability, whereas the rotation shear exerts little influence when flow is small ($\Omega_2 < \gamma_0$) but reduces this stabilizing effect when the rotation flow becomes large enough ($\Omega_2 > \gamma_0$) for low viscosity plasmas ($\tau_R/\tau_V < 1$). However, when the viscosity becomes higher ($\tau_R/\tau_V \gg 1$), the effect of the rotation shear combined with the viscosity appears to be stabilizing. This is consistent with the findings of previous

studies[18-20].

Excluding the toroidal mode coupling effect, the stabilizing effects of the rotation may primarily arise from the equilibrium modifications of the pressure profile, the centrifugal effect and the Coriolis effect due to the toroidal geometry. By artificially turning on/off the time evolution of specific variables (the pressure and the density) in CLT to identify each contribution of these effects and with a simple analytical estimation, we find that the Coriolis effect may have a considerable even dominant influences on the rotation induced stabilization.

The mode structure (or the magnetic island structure) would be distorted as in Ref. 28 and 29, when the rotation shear exists around the rational surfaces, which may be one of illustrations how local flow shear can affect the stability of the tearing mode.

References

1. S. Mirnov, J. Wesley, N. Fujisawa, Y. Gribov, O. Gruber, T. Hender, N. Ivanov, S. Jardin, J. Lister, F. Perkins, M. Rosenbluth, N. Sauthoff, T. Taylor, S. Tokuda, K. Yamazaki, R. Yoshino, A. Bondeson, J. Conner, E. Fredrickson, D. Gates, R. Granetz, R. La Haye, J. Neuhauser, F. Porcelli, D. E. Post, N. A. Uckan, M. Azumi, D. J. Campbell, M. Wakatani, W. M. Nevins, M. Shimada and J. Van Dam, Nuclear Fusion **39** (12), 2251-2389 (1999).
2. T. C. Hender, J. C. Wesley, J. Bialek, A. Bondeson, A. H. Boozer, R. J. Buttery, A. Garofalo, T. P. Goodman, R. S. Granetz, Y. Gribov, O. Gruber, M. Gryaznevich, G. Giruzzi, S. Günter, N. Hayashi, P. Helander, C. C. Hegna, D. F. Howell, D. A. Humphreys, G. T. A. Huysmans, A. W. Hyatt, A. Isayama, S. C. Jardin, Y. Kawano, A. Kellman, C. Kessel, H. R. Koslowski, R. J. L. Haye, E. Lazzaro, Y. Q. Liu, V. Lukash, J. Manickam, S. Medvedev, V. Mertens, S. V. Mirnov, Y. Nakamura, G. Navratil, M. Okabayashi, T. Ozeki, R. Paccagnella, G. Pautasso, F. Porcelli, V. D. Pustovitov, V. Riccardo, M. Sato, O. Sauter, M. J. Schaffer, M. Shimada, P. Sonato, E. J. Strait, M. Sugihara, M. Takechi, A. D. Turnbull, E. Westerhof, D. G. Whyte, R. Yoshino, H. Zohm, t. I. M. H. D. D. Group and Magnet, Nuclear Fusion **47** (6), S128-S202 (2007).
3. R. White, Reviews of Modern Physics **58** (1), 183-207 (1986).
4. H. Zohm, G. Gantenbein, G. Giruzzi, S. Gunter, F. Leuterer, M. Maraschek, J. Meskat, A. G. Peeters, W.

Suttrop, D. Wagner, M. Zabiego, A. U. Team and E. Grp, Nuclear Fusion **39** (5), 577-580 (1999).

5.   Q. Yu, X. D. Zhang and S. Gunter, Physics of Plasmas **11** (5), 1960-1968 (2004).

6.   C. C. Hegna, Physics of Plasmas **5** (5), 1767 (1998).

7.   R. J. La Haye, Physics of Plasmas **13** (5), 055501 (2006).

8.   R. J. Buttery, R. J. La Haye, P. Gohil, G. L. Jackson, H. Reimerdes, E. J. Strait and D.-D. T. the, Physics of Plasmas **15** (5), 056115 (2008).

9.   S. P. Gerhardt, D. P. Brennan, R. Buttery, R. J. La Haye, S. Sabbagh, E. Strait, M. Bell, R. Bell, E. Fredrickson, D. Gates, B. LeBlanc, J. Menard, D. Stutman, K. Tritz and H. Yuh, Nuclear Fusion **49** (3), 032003 (2009).

10.   R. J. La Haye, D. P. Brennan, R. J. Buttery and S. P. Gerhardt, Physics of Plasmas **17** (5), 056110 (2010).

11.   M. S. Chu, L. Chen, L. J. Zheng, C. Ren and A. Bondeson, Nuclear Fusion **39** (11Y), 2107-2111 (1999).

12.   R. B. Paris, Physics of Fluids **26** (10), 2966 (1983).

13.   X. L. Chen and P. J. Morrison, Physics of Fluids B: Plasma Physics **2** (3), 495 (1990).

14.   K. P. Wessen and M. Persson, Journal of Plasma Physics **45**, 267-283 (1991).

15.   X. L. Chen and P. J. Morrison, Physics of Fluids B: Plasma Physics **4** (4), 845 (1992).

16.   R. B. Paris, A. D. Wood and S. Stewart, Physics of Fluids B: Plasma Physics **5** (3), 1027 (1993).

17.   D. Chandra, A. Sen and P. Kaw, Nuclear Fusion **47** (9), 1238-1243 (2007).

18.   R. Coelho and E. Lazzaro, Physics of Plasmas **14** (1), 012101 (2007).

19.   D. Chandra, A. Sen, P. Kaw, M. P. Bora and S. Kruger, Nuclear Fusion **45** (6), 524-530 (2005).

20.   A. Sen, D. Chandra and P. Kaw, Nuclear Fusion **53** (5), 053006 (2013).

21.   C. Z. Cheng and M. S. Chance, Journal of Computational Physics **71** (1), 124-146 (1987).

22.   H. P. Furth, Physics of Fluids **16** (7), 1054 (1973).

23.   G. Ara, B. Basu, B. Coppi, G. Laval, M. N. Rosenbluth and B. V. Waddell, Ann Phys-New York **112** (2), 443-476 (1978).

24.   R. J. Hastie, T. C. Hender, B. A. Carreras, L. A. Charlton and J. A. Holmes, Physics of Fluids **30** (6), 1756 (1987).

25.   Y. Nishimura, "Finite pressure effects on the tokamak sawtooth crash", PhD dissertation at University of Wisconsin, Madison (1998).

26.   W. Shen, G. Y. Fu, Z. M. Sheng, J. A. Breslau and F. Wang, Physics of Plasmas **21** (9) (2014).

27.   E. Frieman and M. Rotenberg, Reviews of Modern Physics **32** (4), 898-902 (1960).

28.   C. Ren, M. S. Chu and J. D. Callen, Physics of Plasmas **6** (4), 1203-1207 (1999).

29.   R. J. La Haye and R. J. Buttery, Physics of Plasmas **16** (2), 022107 (2009).